iments[1,2,9]. No electrons were observed above 40 MeV on the spectrometer phosphor screen (detection threshold 10^7 electrons). Plasma density was independently optimized for the unchannelled accelerator, and highest charge and electron energies were obtained at $4 \times 10^{19}\,\mathrm{cm}^{-3}$. The high density allowed acceleration before the laser diffracted since self modulation and dephasing both occur more quickly at high density, but this also reduced the peak energy compared to the channelled case. Operating the unchannelled accelerator at the density used for the channelled accelerator ($2 \times 10^{19}\,\mathrm{cm}^{-3}$) produced low-charge low-energy beams, since the intensity of the drive beam was not maintained for sufficient distance to allow acceleration at this density without channelling. Using a 600-μm-long plasma at $4 \times 10^{19}\,\mathrm{cm}^{-3}$, which is close to the dephasing length observed in PIC simulations at this density, the unchannelled accelerator produced the same peak energy as in the 2 mm plasma, but with more structure in the spectrum. These results confirm that matching accelerator length to dephasing length is critical for structuring the spectrum, and that extending the length (for instance, using a channel at lower density) results in higher energies.

To differentiate the effects of channelling from pre-ionization, the igniter pulse was fired 80 ps before the drive pulse. The plasma does not expand significantly over 80 ps, so there was no shock wave and the transverse density profile was flat and had no guiding properties. We observed no difference between the drive pulse only and pre-ionized cases, indicating that channelling and not pre-ionization was responsible for differences in the electron beams described above.

The beams from channel-guided accelerators such as those described here, with a few times 10^9 electrons in per cent level energy spread and mrad divergence, as well as intrinsic synchronization to the laser beam, open up a new class of experiments with laser accelerators. The channelling technology offers the ability to control the laser beam propagation much as a copper structure provides guiding and field shaping to RF accelerators. The investment of power in channel formation is less than 5% of the drive pulse power (20% of the energy), yet the spectral density of these beams near 80 MeV is at least a factor of 200 above previous unchannelled experiments using several times the laser power, and peak energy observed is comparable[2]. The narrow energy spread of the channel-produced beams is consistent with simulations, which also indicate that the bunch length is near 10 fs. The channel-guided laser accelerator technique will hence allow efficient generation of femtosecond X-rays[10], coherent THz and infrared radiation[13,30], and is an essential step towards the development of compact multistage electron accelerators with ultrafast bunches and with focusability and luminosity competitive with state of the art RF accelerators. □

Received 4 June; accepted 29 July 2004; doi:10.1038/nature02900.

1. Modena, A. *et al.* Electron acceleration from the breaking of relativistic plasma waves. *Nature* **377,** 606–608 (1995).
2. Malka, V. *et al.* Electron acceleration by a wake field forced by an intense ultrashort laser pulse. *Science* **298,** 1596–1600 (2002).
3. Leemans, W. P. *et al.* Electron-yield enhancement in a laser-wakefield accelerator driven by asymmetric laser pulses. *Phys. Rev. Lett.* **89,** 174802 (2002).
4. Tajima, T. & Dawson, J. M. Laser electron accelerator. *Phys. Rev. Lett.* **43,** 267–270 (1979).
5. Esarey, E., Sprangle, P., Krall, J. & Ting, A. Overview of plasma-based accelerator concepts. *IEEE Trans. Plasma Sci.* **24,** 252–288 (1996).
6. Esarey, E., Krall, J. & Sprangle, P. Envelope analysis of intense laser pulse self-modulation in plasmas. *Phys. Rev. Lett.* **72,** 2887–2890 (1994).
7. Esarey, E., Sprangle, P., Krall, J. & Ting, A. Self-focusing and guiding of short laser pulses in ionizing gases and plasmas. *IEEE J. Quant. Electron.* **33,** 1879–1914 (1997).
8. Najmudin, Z. *et al.* Self-modulated wakefield and forced laser wakefield acceleration of electrons. *Phys. Plasmas* **10,** 2071–2077 (2003).
9. Leemans, W. P. *et al.* Gamma-neutron activation experiments using laser wakefield accelerators. *Phys. Plasmas* **8,** 2510–2516 (2001).
10. Leemans, W. P. *et al.* Observation of terahertz emission from a laser-plasma accelerated electron bunch crossing a plasma-vacuum boundary. *Phys. Rev. Lett.* **91,** 074802 (2003).
11. Catravas, P., Esarey, E. & Leemans, W. P. Femtosecond x-rays from Thomson scattering using laser wakefield accelerators. *Meas. Sci. Technol.* **12,** 1828–1834 (2001).
12. Wang, X. J., Qiu, X. & Ben-Zvi, I. Experimental observation of high-brightness microbunching in a photocathode RF electron gun. *Phys. Rev. E* **54,** R3121–R3124 (1996).
13. Schoenlein, R. W. *et al.* Femtosecond X-ray pulses at 0.4 Å generated by 90° Thomson scattering — A tool for probing the structural dynamics of materials. *Science* **274,** 236–238 (1996).
14. Sprangle, P., Esarey, E., Krall, J. & Joyce, G. Propagation and guiding of intense laser pulses in plasmas. *Phys. Rev. Lett.* **69,** 2200–2203 (1992).
15. Leemans, W. P. *et al.* Plasma guiding and wakefield generation for second-generation experiments. *IEEE Trans. Plasma Sci.* **24,** 331–342 (1996).
16. Umstadter, D., Kim, J. K. & Dodd, E. Laser injection of ultrashort electron pulses into wakefield plasma waves. *Phys. Rev. Lett.* **76,** 2073–2076 (1996).
17. Esarey, E., Hubbard, R. F., Leemans, W. P., Ting, A. & Sprangle, P. Electron injection into plasma wake fields by colliding laser pulses. *Phys. Rev. Lett.* **79,** 2682–2685 (1997).
18. Durfee, C. G. & Milchberg, H. M. Light pipe for high intensity laser pulses. *Phys. Rev. Lett.* **71,** 2409–2412 (1993).
19. Volfbeyn, P., Esarey, E. & Leemans, W. P. Guiding of laser pulses in plasma channels created by the ignitor-heater technique. *Phys. Plasmas* **6,** 2269–2277 (1999).
20. Kim, K. Y., Alexeev, I., Fan, J., Parra, E. & Milchberg, H. M. Plasma waveguides: Addition of end funnels and generation in clustered gases. *AIP Conf. Proc.* **647,** 646–653 (2002).
21. Gaul, E. W. *et al.* Production and characterization of a fully ionized He plasma channel. *Appl. Phys. Lett.* **77,** 4112–4114 (2000).
22. Toth, C. *et al.* Powerful, pulsed, THz radiation from laser accelerated relativistic electron bunches. *Proc. SPIE* **5448,** 491–504 (2004).
23. Leemans, W. P. *et al.* Laser-driven plasma-based accelerators — Wakefield excitation, channel guiding, and laser triggered particle injection. *Phys. Plasmas* **5,** 1615–1623 (1998).
24. Strickland, D. & Mourou, G. Compression of amplified chirped optical pulses. *Opt. Commun.* **56,** 219–221 (1985).
25. Leemans, W. P. *et al.* Terahertz radiation from laser accelerated electron bunches. *Phys. Plasmas* **5,** 2899–2906 (2004).
26. Nieter, C. & Cary, J. R. VORPAL: A versatile plasma simulation code. *J. Comput. Phys.* **196,** 448–473 (2004).
27. Katsouleas, T., Wilks, S., Chen, S., Dawson, J. M. & Su, J. J. Beam loading in plasma accelerators. *Part. Accel.* **22,** 81–99 (1987).
28. Reitsma, A. J. W. *et al.* Simulation of electron postacceleration in a two-stage laser wakefield accelerator. *Phys. Rev. ST Accel. Beams* **5,** 051301 (2002).
29. Tsung, F. S. *et al.* Near GeV energy laser wakefield acceleration of self-injected electrons in a cm scale plasma channel. *Phys. Rev. Lett.* submitted.
30. Saes, M. *et al.* A setup for ultrafast time-resolved x-ray absorption spectroscopy. *Rev. Sci. Instrum.* **75,** 24–30 (2004).

Acknowledgements This work was supported by the US Department of Energy and the National Science Foundation and used resources of the National Energy Research Scientific Computing Center at LBNL; C.G. was also supported by the Hertz Foundation. C.G. acknowledges his faculty advisor J. Wurtele. We appreciate contributions from G. Dugan, J. Faure, G. Fubiani, B. Nagler, K. Nakamura, N. Saleh, B. Shadwick, L. Archambault, M. Dickinson, S. Dimaggio, D. Syversrud, J. Wallig and N. Ybarrolaza.

Competing interests statement The authors declare that they have no competing financial interests.

Correspondence and requests for materials should be addressed to W.P.L. (wpleemans@lbl.gov).

A laser–plasma accelerator producing monoenergetic electron beams

J. Faure[1], Y. Glinec[1], A. Pukhov[2], S. Kiselev[2], S. Gordienko[2], E. Lefebvre[3], J.-P. Rousseau[1], F. Burgy[1] & V. Malka[1]

[1]*Laboratoire d'Optique Appliquée, Ecole Polytechnique, ENSTA, CNRS, UMR 7639, 91761 Palaiseau, France*
[2]*Institut fur Theoretische Physik, 1, Heinrich-Heine-Universitat Duesseldorf, 40225 Duesseldorf, Germany*
[3]*Département de Physique Théorique et Appliquée, CEA/DAM Ile-de-France, 91680 Bruyères-le-Châtel, France*

Particle accelerators are used in a wide variety of fields, ranging from medicine and biology to high-energy physics. The accelerating fields in conventional accelerators are limited to a few tens of MeV m^{-1}, owing to material breakdown at the walls of the structure. Thus, the production of energetic particle beams currently requires large-scale accelerators and expensive infrastructures. Laser–plasma accelerators[1] have been proposed as a next generation of compact accelerators because of the huge

electric fields they can sustain[2–5] (>100 GeV m^{-1}). However, it has been difficult to use them efficiently for applications because they have produced poor-quality particle beams with large energy spreads[2–10], owing to a randomization of electrons in phase space. Here we demonstrate that this randomization can be suppressed and that the quality of the electron beams can be dramatically enhanced. Within a length of 3 mm, the laser drives a plasma bubble[11] that traps and accelerates plasma electrons. The resulting electron beam is extremely collimated and quasi-monoenergetic, with a high charge of 0.5 nC at 170 MeV.

For most practical applications, high-quality particle beams with high spatial quality and monoenergetic energy distribution are required. A beam that does not satisfy these criteria would be hard to use, because it would be difficult to transport it and/or to focus it. In order to produce high-quality beams from plasma-based accelerators, two challenges have to be met: (1) the generation of an accelerating structure in the plasma, and (2) the trapping and acceleration of injected beam loads into the accelerating structure. In order to generate accelerating structures in the plasma, a focused ultraintense laser pulse is used to drive large-amplitude plasma waves. One possible method for achieving this is the laser wakefield, in which plasma waves are excited by the laser ponderomotive force. When the laser pulse length $c\tau$ (where c is the speed of light and τ is the pulse duration) is comparable to the plasma wavelength λ_p, the ponderomotive force, which is proportional to the gradient of the laser intensity, efficiently pushes plasma electrons out of the regions of strong laser field. Thus, electrons are separated from the ions, which do not move because of their higher mass. This creates the space charge field needed for particle acceleration, that is, the plasma wave.

The generation of intense accelerating fields in plasmas has been demonstrated in many experiments[8,12,13]. Proof-of-principle experiments have shown the feasibility of externally injecting electrons from a conventional accelerator into the laser-driven plasma accelerating structure[8–10]. However, the output beam quality has been poor: the electron energy distribution has had a 100% energy spread. Until now, the most widespread method for producing electron beams from plasmas has relied on the self-modulated laser wakefield accelerator[14–16]. In this accelerator, the laser pulse is longer than the plasma wavelength. Under the influence of the self-modulation instability, its envelope modulates at the plasma frequency and resonantly excites a plasma wave. When the plasma wave amplitude reaches the wave-breaking level, copious amounts of plasma background electrons are trapped in the plasma wave and accelerated. Numerous experiments have produced electron beams with nC charge and divergence varying from a few degrees to tens of degrees and maxwellian energy distributions[2–4]. More recently, several groups[5–7,17] have demonstrated that more compact lasers can be used to efficiently generate high-repetition-rate (10 Hz) electron sources, which could be used for applications. However, these beams still have very large energy spreads and a low number of electrons at high energy (typically <1 pC at 200 ± 10 MeV). Previous experiments inherently produced poor-quality beams: wave-breaking occurred under the laser pulse envelope and the accelerated electrons were also under the influence of the ultraintense laser field. Direct laser acceleration[6,18] by transverse laser field caused the spatial beam quality to deteriorate, causing emittance growth.

Here we demonstrate the generation of high-quality electron beams from ultraintense laser–plasma acceleration. Extremely collimated beams with 10 mrad divergence and 0.5 ± 0.2 nC of charge at 170 ± 20 MeV have been produced. Contrary to all previous results obtained from laser–plasma accelerators, the electron energy distribution is quasi-monoenergetic. The number of high-energy electrons (170 MeV) is increased by at least three orders of magnitude with respect to previous work.

The experiment was performed by focusing a chirped pulse amplification laser[19,20] onto a helium gas jet (Fig. 1). Figure 2a shows a picture of the electron beam when no magnetic field is applied. The electron beam is very well collimated, with a 10 mrad divergence (full-width at half-maximum, FWHM); to our knowl-

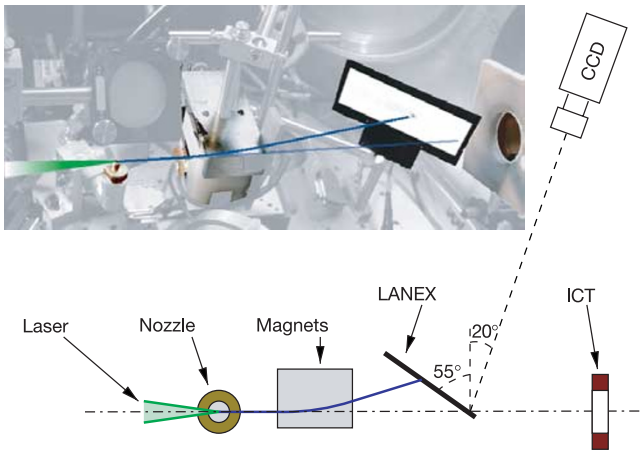

Figure 1 Experimental set-up. Top, picture of the experiment; bottom, diagram. An ultrashort and ultraintense laser pulse is focused onto a 3 mm supersonic gas jet and produces a highly collimated 170 MeV electron beam. LANEX is a phosphor screen; CCD, charge-coupled device camera; ICT, integrating current transformer.

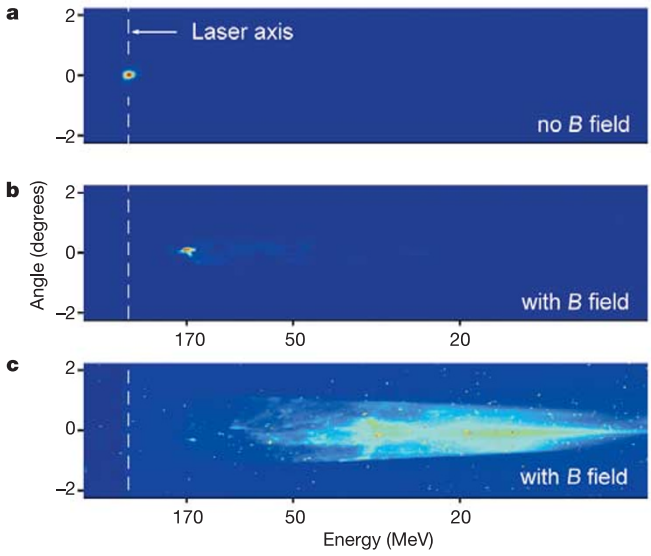

Figure 2 Raw images obtained on the LANEX screen. The vertical axis represents the beam angular divergence. When a magnetic field is applied, the horizontal axis represents electron energy. The white vertical dashed line is drawn at the intersection of the laser axis with the LANEX screen. **a**, Image of the electron beam spatial distribution obtained from the LANEX screen when no magnetic field (B) is applied. **b**, Image obtained when the magnetic field is applied, showing that the bulk of the beam is deviated and its position corresponds to 170 MeV electrons. The fact that the beam trajectory is displaced when a magnetic field is applied confirms that the signal on the LANEX screen corresponds to electrons and not to photons. **c**, Image obtained with a magnetic field and a higher plasma density ($n_e = 2 \times 10^{19}$ cm^{-3}). This electron beam has a much larger divergence and a 100% energy spread with few electrons above 100 MeV.

edge, this is the smallest divergence ever measured for a beam emerging from a plasma accelerator. Figure 2b shows the deviation of the beam when a magnetic field is applied. The image shows a narrow peak around 170 MeV, indicating efficient monoenergetic acceleration. For comparison, Fig. 2c shows an image obtained at higher electron density in the plasma ($n_e = 2 \times 10^{19}\,\mathrm{cm}^{-3}$). Here, electrons are randomly accelerated to all energies and the number of high-energy electrons is low. In addition, the beam divergence is much larger than in Fig. 2b. Figure 3 shows an electron spectrum after deconvolution. The distribution is clearly quasi-monoenergetic and peaks at 170 MeV, with a 24% energy spread (corresponding to the spectrometer resolution).

Finally, the charge contained in this beam can be inferred using an integrating current transformer: the whole beam contains 2 ± 0.5 nC, and the charge at 170 ± 20 MeV is 0.5 ± 0.2 nC. From the above, we can deduce that the electron beam energy was 100 mJ. Thus, the energy conversion from the laser to the electron beam was 10%.

Experimentally, this regime could be reached in a narrow range of parameters: stretching the pulse duration above 50 fs was sufficient to lose the peaked energy distribution. Similarly, when the electron density was increased from $6 \times 10^{18}\,\mathrm{cm}^{-3}$ to $7.5 \times 10^{18}\,\mathrm{cm}^{-3}$, the energy distribution became a broad plateau, similar to previous results[5]. Above $10^{19}\,\mathrm{cm}^{-3}$, the electron distribution was maxwellian-like with very few electrons accelerated at high energy. Below $6 \times 10^{18}\,\mathrm{cm}^{-3}$, the number of accelerated electrons decreased dramatically, although the distribution was still mono-energetic. The evolution of electron spectra with experimental parameters indicates that using laser pulses shorter than the plasma period is beneficial for high-quality and monoenergetic electron acceleration.

To reach a deeper understanding of the experiment, we have run three-dimensional (3D) particle-in-cell (PIC) simulations using the code Virtual Laser Plasma Laboratory[21]. The simulation results are shown in Fig. 4a–c. The simulation suggests that our experimental results can be explained by the following scenario. (1) At the beginning of the simulation, the laser pulse length (9 μm) is nearly resonant with the plasma wave ($\lambda_p = 13.6\,\mu\mathrm{m}$); but its diameter ($21\,\mu\mathrm{m} > \lambda_p$) is larger than the matched diameter. (2) As the pulse propagates in the plateau region of the gas jet, it self-focuses and undergoes longitudinal compression by plasma waves (Fig. 4a). This decreases the effective radius of the laser pulse and increases the

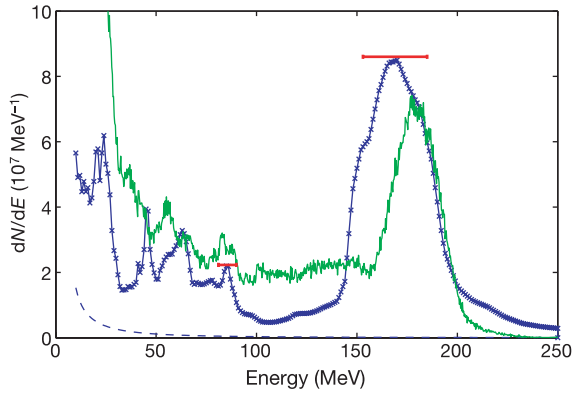

Figure 3 Experimental and simulated electron spectra. Blue line with crosses, electron spectrum corresponding to Fig. 2b, after deconvolution. Dashed line, estimation of the background level. Red horizontal error bars, resolution of the spectrometer. Green line, electron spectrum obtained from 3D PIC simulations. d*N*/d*E* is the number of electrons per MeV (*E* is the electron energy in MeV).

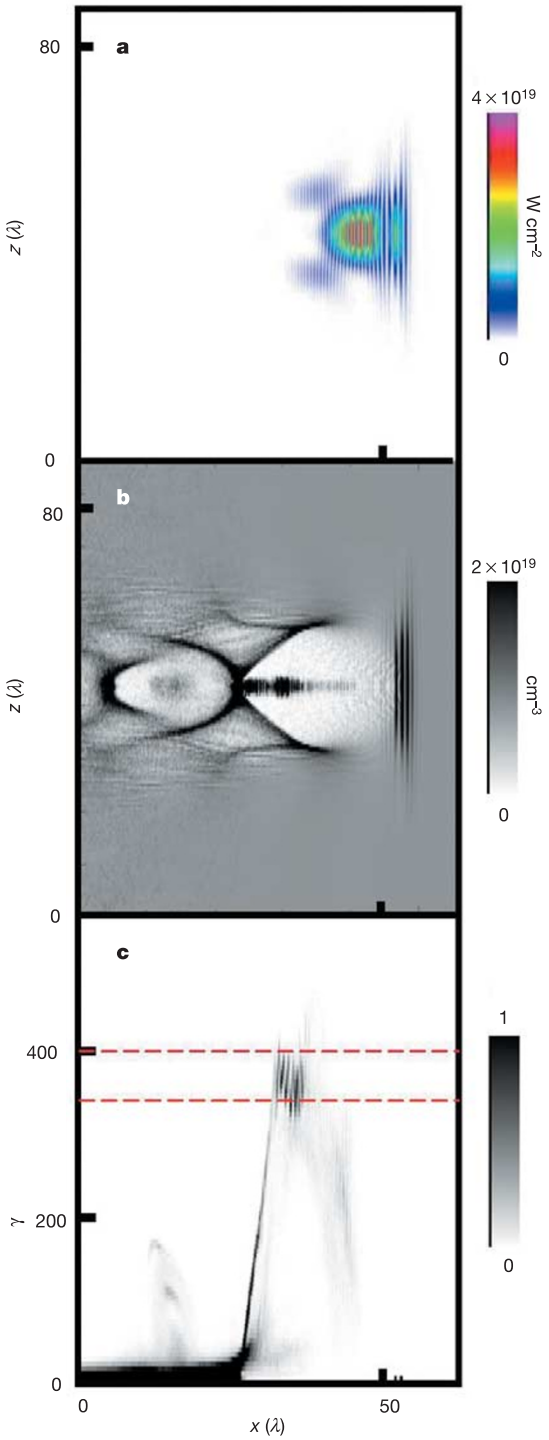

Figure 4 3D PIC simulation results. **a**, **b**, Distributions of laser intensity (**a**) and electron density (**b**) in the *x*–*z* plane, which is perpendicular to the polarization direction and passes through the laser axis. The laser pulse runs from left to right, and has propagated 2 mm in the plasma. The bubble structure is clearly visible. The laser pushes the electron fluid forward at the bubble head and creates a density compression there. Behind the laser we see the cavitated region with nearly zero electron density. The radially expelled electrons flow along the cavity boundary and collide at the X-point at the bubble base. Some electrons are trapped and accelerated in the bubble. The beam of accelerated electrons is seen as the black rod in **b**. These electrons are propagating behind the laser pulse (**a**) and are not disturbed by the laser field. **c**, Electron phase space density $f(x,\gamma)$ in arbitrary units. γ is the relativistic factor of the electron: $\gamma = (1 - v^2/c^2)^{-1/2}$, and v is the electron velocity. We see that the electrons have dephased and have self-bunched in the phase space around $\gamma \gg 350$. This self-bunching results in the mono-energetic peak in the energy spectrum (Fig. 3). The red horizontal dashed lines indicate the location of the mono-energetic peak in the phase space.

laser intensity by one order of magnitude. (3) This compressed laser pulse is now resonant with the plasma wave and it drives a highly nonlinear wakefield (Fig. 4b): the laser ponderomotive potential expels the plasma electrons radially and leaves a cavitated region behind (this is referred to as the 'cavitation' or 'blow-out' regime). In this regime, the 3D structure of the wakefield resembles a plasma bubble[11]. (4) As the electron density at the walls of the bubble becomes large, wave-breaking occurs and electrons are injected and accelerated inside the bubble. (5) As the number of trapped electrons increases, the bubble elongates. Its effective group velocity decreases, and electrons start to dephase with respect to the accelerating field. This dephasing causes electron self-bunching in the phase space (Fig. 4c). This self-bunching results in the monoenergetic peak in the energy spectrum (Fig. 3).

Simulations also show that the quality of the electron beam is higher when trapped electrons do not interact with the laser field. If this were to occur, the laser field would cause the electrons to scatter in phase space, degrading the low divergence as well as the monoenergetic distribution. This argument could explain why higher-quality beams are obtained experimentally for shorter pulses and lower electron densities.

Figure 4a shows that the self-focused and compressed laser pulse stands in front of the trapped electrons (Fig. 4b), leaving them almost undisturbed[5,11]. The electron energy spectrum obtained from the simulations is shown in Fig. 3: it peaks at 175 ± 25 MeV, in agreement with the experiment. The divergence of 10 mrad is also in agreement with experiments. Simulations also indicate that the electron bunch duration is less than 30 fs (here, the term 'bunch' refers to the fact that electrons are created in short bursts). Because the electron distribution is quasi-monoenergetic, the bunch will stay short upon propagation: considering a 24% energy spread at 170 MeV, we can show that the bunch stretches by only 50 fs m^{-1} as it propagates.

Another important point is the apparent robustness of the 'blow-out' regime. The initial laser parameters—for example, the focal spot radius and intensity—were far from the final values in the bubble (Fig. 4). Yet self-focusing led to compression of the laser pulse and to the formation of an electron cavity. The energy of 1 J for a 30 fs laser pulse, as used in the experiment, seems to be close to the threshold for this regime. Simulations[11] suggest that with more laser energy and shorter pulses, the blow-out regime and the formation of the bubble will lead to the acceleration of monoenergetic beams at higher energies and higher charges.

Our experimental results and 3D PIC simulations indicate that it is possible to generate a monoenergetic electron beam by carefully selecting laser and plasma parameters. The bunch duration (<50 fs), along with the present improvement in the charge (nC) and the quality of the electron beam (monoenergetic spectrum, low divergence), reinforce the relevance of plasma-based accelerators for many applications (such as high-resolution radiography for non-destructive material inspection, radiotherapy, ultrafast chemistry, radiobiology and material science). With the rapid progress of laser science, we expect that it will soon become possible to generate compact, monoenergetic and high-quality electron beams with a tunable energy range at a reasonable cost. Such a source would be perfectly adapted as an injector for future GeV laser–plasma accelerator schemes. It would also be relevant for generating ultrashort X-ray sources, using undulators or lasers via Thomson scattering. □

Methods

Laser

This new regime was reached by using the ultrashort and ultraintense laser pulse generated in a titanium-doped sapphire, chirped pulse amplification laser system. The laser pulse had a 33 ± 2 fs duration (FWHM), and contained 1 J of laser energy at central wavelength 820 nm. It was focused onto the edge of a 3-mm-long supersonic helium gas jet using a *f*/18 off-axis parabola. The diffraction-limited focal spot had a diameter of $r_0 = 21\,\mu m$ at FWHM, producing a vacuum-focused laser intensity of $I = 3.2 \times 10^{18}\,W\,cm^{-2}$, for which the corresponding normalized potential vector is $a_0 = eA/(mc^2) = 1.3$ (A is the laser vector potential, e and m are respectively the charge and mass of the electron). For these high laser intensities, the helium gas was fully ionized by the foot of the laser pulse and ionization did not play a role in the interaction.

Electron diagnostics

Electron detection was achieved using a LANEX phosphor screen, placed 25 cm after the gas jet. As electrons passed through the screen, energy was deposited and re-emitted into visible photons which were then imaged onto a 16 bit charge-coupled device (CCD) camera. For energy distribution measurements, a 0.45 T, 5-cm-long permanent magnet was inserted between the gas jet and the LANEX screen. The LANEX screen was protected by a 100-μm-thick aluminium foil in order to avoid direct exposure to the laser light. For deconvolution of the images obtained with the LANEX screen, electron deviation in the magnetic field has been considered as well as the electron stopping power inside the LANEX screen. The resolution (red error bar in Fig. 3) is limited by the electron beam spatial quality and by the dispersing power of the magnet. This gives a resolution of respectively 32 MeV and 12 MeV for 170 MeV and 100 MeV energies. Above 200 MeV, the resolution quickly degrades. The charge of the electron beam was measured using an integrating current transformer placed 30 cm behind the LANEX screen. It allowed us to measure the total charge of the beam when no magnetic field was applied, and the charge above 100 MeV when the magnetic field was applied.

PIC simulations

The simulation parameters corresponded to the optimal experimental case: the plasma electron density was $n_e = 6 \times 10^{18}\,cm^{-3}$, the laser pulse duration was 30 fs and the initial laser spot size 21 μm FWHM. The laser pulse was assumed to be a perfect gaussian containing 1 J of energy. The plasma profile was chosen to fit the experimental density profile of the gas jet.

Received 5 July; accepted 25 August 2004; doi:10.1038/nature02963.

1. Tajima, T. & Dawson, J. M. Laser electron accelerator. *Phys. Rev. Lett.* **43,** 267–270 (1979).
2. Modena, A. *et al.* Electron acceleration from the breaking of relativistic plasma waves. *Nature* **337,** 606–608 (1995).
3. Umstadter, D., Chen, S.-Y., Maksimchuk, A., Mourou, G. & Wagner, R. Nonlinear optics in relativistic plasmas and laser wake field acceleration of electrons. *Science* **273,** 472–475 (1996).
4. Moore, C. I. *et al.* Electron trapping in self-modulated laser wakefields by Raman backscatter. *Phys. Rev. Lett.* **79,** 3909–3912 (1997).
5. Malka, V. *et al.* Electron acceleration by a wake field forced by an intense ultrashort laser pulse. *Science* **298,** 1596–1600 (2002).
6. Gahn, C. *et al.* Multi-MeV electron beam generation by direct laser acceleration in high-density plasma channels. *Phys. Rev. Lett.* **83,** 4772–4775 (1999).
7. Malka, V. *et al.* Characterization of electron beams produced by ultrashort (30 fs) laser pulses. *Phys. Plasmas* **8,** 2605–2608 (2001).
8. Kitagawa, Y. *et al.* Beat-wave excitation of plasma wave and observation of accelerated electrons. *Phys. Rev. Lett.* **68,** 48–51 (1992).
9. Everett, M. *et al.* Trapped electron acceleration by a laser-driven relativistic plasma wave. *Nature* **368,** 527–529 (1994).
10. Amiranoff, F. *et al.* Observation of laser wakefield acceleration of electrons. *Phys. Rev. Lett.* **81,** 995–998 (1998).
11. Pukhov, A. & Meyer-ter-Vehn, J. Laser wake field acceleration: the highly non-linear broken-wave regime. *Appl. Phys. B* **74,** 355–361 (2002).
12. Clayton, C. E., Joshi, C., Darrow, C. & Umstadter, D. Relativistic plasma-wave excitation by collinear optical mixing. *Phys. Rev. Lett.* **54,** 2343–2346 (1985).
13. Amiranoff, F. *et al.* Observation of modulational instability in Nd-laser beat-wave experiments. *Phys. Rev. Lett.* **68,** 3710–3713 (1992).
14. Andreev, N. E., Gorbunov, L. M., Kirsanov, V. I., Pogosova, A. A. & Ramazashvili, R. R. Resonant excitation of wakefields by a laser pulse in a plasma. *JETP Lett.* **55,** 571–574 (1992).
15. Sprangle, P., Esarey, E., Krall, J. & Joyce, G. Propagation and guiding of intense laser pulses in plasmas. *Phys. Rev. Lett.* **69,** 2200–2203 (1992).
16. Antonsen, T. M. & Mora, P. Self-focusing and Raman scattering of laser pulses in tenuous plasmas. *Phys. Rev. Lett.* **69,** 2204–2207 (1992).
17. Leemans, W. P. *et al.* Electron-yield enhancement in a laser-wakefield accelerator driven by asymmetric laser pulses. *Phys. Rev. Lett.* **89,** 174802 (2002).
18. Pukhov, A., Sheng, Z.-M. & Meyer-ter-Vehn, J. Particle acceleration in relativistic laser channels. *Phys. Plasmas* **6,** 2847–2854 (1999).
19. Strickland, D. & Mourou, G. Compression of amplified chirped optical pulses. *Opt. Commun.* **56,** 219–221 (1985).
20. Pittman, M. *et al.* Design and characterization of a near-diffraction-limited femtosecond 100-TW 10-Hz high-intensity laser system. *Appl. Phys. B* **74,** 529–535 (2002).
21. Pukhov, A. J. Three-dimensional electromagnetic relativistic particle-in-cell code VLPL (Virtual Laser Plasma Lab). *J. Plasma Phys.* **61,** 425–433 (1999).

Acknowledgements We acknowledge support from the European Community Research Infrastructure Activity under the FP6 "Structuring the European Research Area" programme (CARE) and from the German Scientific Council (DFG).

Competing interests statement The authors declare that they have no competing financial interests.

Correspondence and requests for materials should be addressed to V.M. (victor.malka@ensta.fr).